Multiplicity dependence of pion, kaon, proton and lambda production in p–Pb collisions at $\sqrt{s_{NN}} = 5.02$ TeV

ALICE Collaboration*

ARTICLE INFO

ABSTRACT

In this Letter, comprehensive results on $\pi^{\pm}$, $K^{\pm}$, K^0_S, $p(\bar{p})$ and $\Lambda(\bar{\Lambda})$ production at mid-rapidity ($0 < y_{CMS} < 0.5$) in p–Pb collisions at $\sqrt{s_{NN}} = 5.02$ TeV, measured by the ALICE detector at the LHC, are reported. The transverse momentum distributions exhibit a hardening as a function of event multiplicity, which is stronger for heavier particles. This behavior is similar to what has been observed in pp and Pb–Pb collisions at the LHC. The measured p_T distributions are compared to d–Au, Au–Au and Pb–Pb results at lower energy and with predictions based on QCD-inspired and hydrodynamic models.

1. Introduction

High-energy heavy-ion (AA) collisions offer a unique possibility to study nuclear matter under extreme conditions, in particular the deconfined quark–gluon plasma which has been predicted by quantum chromodynamics (QCD) [1–4]. The interpretation of heavy-ion results depends crucially on the comparison with results from smaller collision systems such as proton–proton (pp) or proton–nucleus (pA).

The bulk matter created in high-energy nuclear reactions can be quantitatively described in terms of hydrodynamic and statistical models. The initial hot and dense partonic matter rapidly expands and cools down, ultimately undergoing a transition to a hadron gas phase [5]. The observed ratios of particle abundances can be described in terms of statistical models [6,7], which are governed mainly by two parameters, the chemical freeze-out temperature T_{ch} and the baryochemical potential μ_B which describes the net baryon content of the system. These models provide an accurate description of the data over a large range of center-of-mass energies (see e.g. [8]), but a surprisingly large deviation (about 50%) was found for the proton production yield at the LHC [9,10]. During the expansion phase, collective hydrodynamic flow develops from the initially generated pressure gradients in the strongly interacting system. This results in a characteristic dependence of the shape of the transverse momentum (p_T) distribution on the particle mass, which can be described with a common kinetic freeze-out temperature parameter T_{kin} and a collective average expansion velocity $\langle \beta_T \rangle$ [11].

Proton–nucleus (pA) collisions are intermediate between proton–proton (pp) and nucleus–nucleus (AA) collisions in terms of system size and number of produced particles. Comparing particle production in pp, pA, and AA reactions has frequently been used to separate initial state effects, linked to the use of nuclear beams or targets, from final state effects, linked to the presence of hot and dense matter. At the LHC, however, the pseudo-rapidity density of final state particles in pA collisions reaches values which can become comparable to semi-peripheral Au–Au ($\sim$60% most central) and Cu–Cu ($\sim$30% most central) collisions at top RHIC energy [12]. Therefore the assumption that final state dense matter effects can be neglected in pA may no longer be valid. In addition, pA collisions allow for the investigation of fundamental properties of QCD: the relevant part of the initial state nuclear wave function extends to very low fractional parton momentum x and very high gluon densities, where parton shadowing and novel phenomena like saturation, e.g. as implemented in the Color Glass Condensate model (CGC), may become apparent [13,14].

Recently, measurements at the LHC in high multiplicity pp and p–Pb collisions have revealed a near-side long-range "ridge" structure in the two-particle correlations [15,16]. The observation of an unexpected "double-ridge" structure in the two-particle correlations in high multiplicity p–Pb collisions has also been reported [17–20]. This is flat and long-range in pseudo-rapidity $\Delta\eta$ and modulated in azimuth approximately like $\cos(2\Delta\phi)$, where $\Delta\eta$ and $\Delta\phi$ are the differences in pseudo-rapidity η and azimuthal angle ϕ between the two particles. Various mechanisms have been proposed to explain the origin of this double-ridge like structure. Both a CGC description [21], based on initial state nonlinear gluon interactions, as well as a model based on hydrodynamic flow [22, 23], assuming strong interactions between final state partons or hadrons, can give a satisfactory description of the p–Pb correlation data. However, the modeling of small systems such as p–Pb

* *E-mail address:* alice-publications@cern.ch.

is complicated because uncertainties related to initial state geometrical fluctuations play a large role and because viscous corrections may be too large for hydrodynamics to be a reliable framework [24]. Additional experimental information is therefore required to reveal the origin of these correlations. The p_T distributions and yields of particles of different mass at low and intermediate momenta of less than a few GeV/c (where the vast majority of particles is produced) can provide important information about the system created in high-energy hadron reactions.

Previous results on identified particle production in pp [25–29] and Pb–Pb [9,10] collisions at the LHC have been reported. In this Letter we report on the measurement of $\pi^\pm$, $K^\pm$, K^0_S, p($\bar{p}$) and $\Lambda(\bar{\Lambda})$ production as a function of the event multiplicity in p–Pb collisions at a nucleon–nucleon center-of-mass energy $\sqrt{s_{NN}} = 5.02$ TeV. The results are presented over the following p_T ranges: 0.1–3, 0.2–2.5, 0–8, 0.3–4 and 0.6–8 GeV/c for $\pi^\pm$, $K^\pm$, K^0_S, p($\bar{p}$) and $\Lambda(\bar{\Lambda})$, respectively. Results on π, K, p production in p–Pb collisions have been recently reported by the CMS Collaboration [30].

2. Sample and data analysis

The results presented in this Letter are obtained from a sample of the data collected during the LHC p–Pb run at $\sqrt{s_{NN}} = 5.02$ TeV in the beginning of 2013. Because of the 2-in-1 magnet design of the LHC [31], the energy of the two beams cannot be adjusted independently and is 4 ZTeV, leading to different energies due to the different Z/A. The nucleon–nucleon center-of-mass system, therefore, was moving in the laboratory frame with a rapidity of $y_{NN} = -0.465$ in the direction of the proton beam. The number of colliding bunches was varied from 8 to 288. The total number of protons and Pb ions in the beams ranged from 0.2×10^{12} to 6.5×10^{12} and from 0.1×10^{12} to 4.4×10^{12}, respectively. The maximum luminosity at the ALICE interaction point was for the data used in this Letter 5×10^{27} cm^{-2} s^{-1} resulting in a hadronic interaction rate of 10 kHz. The interaction region had an r.m.s. of 6.3 cm along the beam direction and of about 60 μm in the direction transverse to the beam. For the results presented in this Letter, a low-luminosity data sample has been analyzed where the event pile-up rate has been estimated to have negligible effects on the results. The integrated luminosity corresponding to the used data sample was about 14 μb^{-1} (7 μb^{-1}) for the neutral (charged) hadron analysis. The LHC configuration was such that the lead beam circulated in the "counter-clockwise" direction, corresponding to the ALICE A direction or positive rapidity as per the convention used in this Letter.

A detailed description of the ALICE apparatus can be found in [32]. The minimum-bias trigger signal was provided by the VZERO counters, two arrays of 32 scintillator tiles each covering the full azimuth within $2.8 < \eta_{lab} < 5.1$ (VZERO-A, Pb beam direction) and $-3.7 < \eta_{lab} < -1.7$ (VZERO-C, p beam direction). The signal amplitude and arrival time collected in each tile were recorded. A coincidence of signals in both VZERO-A and VZERO-C detectors was required to remove contamination from single diffractive and electromagnetic events [33]. The time resolution is better than 1 ns, allowing discrimination of beam–beam collisions from background events produced outside of the interaction region. In the offline analysis, background was further suppressed by the time information recorded in two neutron Zero Degree Calorimeters (ZDCs), which are located at $+112.5$ m (ZNA) and -112.5 m (ZNC) from the interaction point. A dedicated quartz radiator Cherenkov detector (T0) provided a measurement of the event time of the collision.

The ALICE central-barrel tracking detectors cover the full azimuth within $|\eta_{lab}| < 0.9$. They are located inside a solenoidal

Table 1
Definition of the event classes as fractions of the analyzed event sample and their corresponding $\langle dN_{ch}/d\eta \rangle$ within $|\eta_{lab}| < 0.5$ (systematic uncertainties only, statistical uncertainties are negligible).

Event class	V0A range (arb. unit)	$\langle dN_{ch}/d\eta \rangle$ $\|\eta_{lab}\| < 0.5$
0–5%	>227	45 ± 1
5–10%	187–227	36.2 ± 0.8
10–20%	142–187	30.5 ± 0.7
20–40%	89–142	23.2 ± 0.5
40–60%	52–89	16.1 ± 0.4
60–80%	22–52	9.8 ± 0.2
80–100%	<22	4.4 ± 0.1

magnet providing a magnetic field of 0.5 T. The innermost barrel detector is the Inner Tracking System (ITS). It consists of six layers of silicon devices grouped in three individual detector systems which employ different technologies (from the innermost outwards): the Silicon Pixel Detector (SPD), the Silicon Drift Detector (SDD) and the Silicon Strip Detector (SSD). The Time Projection Chamber (TPC), the main central-barrel tracking device, follows outwards. Finally the Transition Radiation Detector (TRD) extends the tracking farther away from the beam axis. The primary vertex position was determined separately in the SPD [33] and from tracks reconstructed in the whole central barrel (global tracks). The events were further selected by requiring that the longitudinal position of the primary vertex was within 10 cm of the nominal interaction point and that the vertices reconstructed from SPD tracklets and from global tracks are compatible. In total from a sample of 29.8 (15.3) million triggered events about 24.7 (12.5) million events passing the selection criteria were used in the neutral (charged) hadron analysis.

In order to study the multiplicity dependence, the selected event sample was divided into seven event classes, based on cuts on the total charge deposited in the VZERO-A detector (V0A). The corresponding fractions of the data sample in each class are summarized in Table 1. The mean charged-particle multiplicity densities ($\langle dN_{ch}/d\eta \rangle$) within $|\eta_{lab}| < 0.5$ corresponding to the different event classes are also listed in the table. These are obtained using the method presented in [33] and are corrected for acceptance and tracking efficiency as well as for contamination by secondary particles. The relative standard deviation of the track multiplicity distribution for the event classes defined in Table 1 ranges from 78% to 29% for the 80–100% and 0–5% classes, respectively. It should be noted that the average multiplicity in the 80–100% bin is well below the corresponding multiplicity in pp minimum-bias collisions [34] and therefore likely to be subject to a strong selection bias. Contrary to our earlier measurement of $\langle dN_{ch}/d\eta \rangle$ [33], the values in Table 1 are not corrected for trigger and vertex-reconstruction efficiency, which is of the order of 2% for NSD events [33]. The same holds true for the p_T distributions, which are presented in the next section.

Charged-hadron identification in the central barrel was performed with the ITS, TPC [35] and Time-Of-Flight (TOF) [36] detectors. The drift and strip layers of the ITS provide a measurement of the specific energy loss with a resolution of about 10%. In a standalone tracking mode, the identification of pions, kaons, and protons is thus extended down to respectively 0.1, 0.2, 0.3 GeV/c in p_T. The TPC provides particle identification at low momenta via specific energy loss dE/dx in the fill gas by measuring up to 159 samples per track with a resolution of about 6%. The separation power achieved in p–Pb collisions is identical to that in pp collisions [37]. Further outwards at about 3.7 m from the beam line, the TOF array allows identification at higher p_T measuring the particle speed with the time-of-flight technique. The total time resolution is about 85 ps for events in the multiplicity classes from 0% to ~80%. In more peripheral collisions, where multiplicities are

similar to pp, it decreases to about 120 ps due to a worse start-time (collision-time) resolution [37]. The start-time of the event was determined by combining the time estimated using the particle arrival times at the TOF and the time measured by the T0 detector [36].

Since the p–Pb center-of-mass system moved in the laboratory frame with a rapidity of $y_{NN} = -0.465$, the nominal acceptance of the central barrel of the ALICE detector was asymmetric with respect to $y_{CMS} = 0$. In order to ensure good detector acceptance and optimal particle identification performance, tracks were selected in the rapidity interval $0 < y_{CMS} < 0.5$ in the nucleon–nucleon center-of-mass system. Event generator studies and repeating the analysis in $|y_{CMS}| < 0.2$ indicate differences between the two rapidity selections smaller than 2% in the normalization and 3% in the shape of the transverse momentum distributions.

In this Letter we present results for primary particles, defined as all particles produced in the collision, including decay products, but excluding weak decays of strange particles. The analysis technique is described in detail in [9,10,38]. Here we briefly review the most relevant points.

Three approaches were used for the identification of $\pi^\pm$, $K^\pm$, and p($\bar{p}$), called "ITS standalone", "TPC/TOF" and "TOF fits" [9,10] in the following. In the "ITS standalone" method, a probability for each particle species is calculated in each layer based on the measured energy loss signal and the known response function. The information from all layers is combined in a bayesian approach with iteratively determined priors. Finally, the type with the highest probability is assigned to the track. This method is used in the p_T ranges $0.1 < p_T < 0.7$ GeV/c, $0.2 < p_T < 0.6$ GeV/c and $0.3 < p_T < 0.65$ GeV/c for $\pi^\pm$, $K^\pm$, and p($\bar{p}$), respectively. In contrast to the analysis in the high multiplicity environment of central heavy-ion collisions, the contribution of tracks with wrongly associated clusters is negligible in p–Pb collisions. In the "TPC/TOF" method, the particle is identified by requiring that its measured dE/dx and time-of-flight are within $\pm 3\sigma$ from the expected values in the TPC and/or TOF. This method is used in the p_T ranges $0.2 < p_T < 1.5$ GeV/c, $0.3 < p_T < 1.3$ GeV/c and $0.5 < p_T < 2.0$ GeV/c for $\pi^\pm$, $K^\pm$, and p($\bar{p}$), respectively. In the third method the TOF time distribution is fitted to extract the yields, with the expected shapes based on the knowledge of the TOF response function for different particle species. This method is used in the p_T range starting from 0.5 GeV/c up to 3, 2.5 and 4 GeV/c for $\pi^\pm$, $K^\pm$, and p($\bar{p}$), respectively. Contamination from secondary particles was subtracted with a data-driven approach, based on the fit of the transverse distance-of-closest approach to the primary vertex (DCA$_{xy}$) distribution with the expected shapes for primary and secondary particles [9,10]. The results of the three analyses were combined using the (largely independent) systematic uncertainties as weights in the overlapping ranges, after checking for their compatibility.

The K^0_S and $\Lambda(\bar{\Lambda})$ particles were identified exploiting their "V^0" weak decay topology in the channels $K^0_S \rightarrow \pi^+\pi^-$ and $\Lambda(\bar{\Lambda}) \rightarrow$ pπ^-($\bar{p}\pi^+$), which have branching ratios of 69.2% and 63.9%, respectively [39]. The selection criteria used to define two tracks as V^0 decay candidates are listed in Table 2 (see [26] for details). Since the cosine of pointing angle (the angle between the particle momentum associated with the V^0 candidate and a vector connecting the primary vertex and the V^0 position [26]) resolution changes significantly with momentum, the value used in the selection is p_T dependent and such that no more than 1% of the primary particle signal is removed.

The typical reconstruction efficiencies (excluding branching ratios) are about 15% at low p_T (~ 0.5 GeV/c), increasing to about 70% for K^0_S and 55% for $\Lambda(\bar{\Lambda})$ at higher momenta ($p_T > 3$ GeV/c). The signal is extracted from the reconstructed invariant mass

Table 2
V^0 topological selection cuts (DCA: distance-of-closest approach).

Selection variable	Cut value
2D decay radius	>0.50 cm
Daughter track DCA to prim. vertex	>0.06 cm
DCA between daughter tracks	$<1.0\sigma$
Cosine of pointing angle (K^0_S)	p_T dependent ($<1\%$ signal loss)
Cosine of pointing angle (Λ and $\bar{\Lambda}$)	p_T dependent ($<1\%$ signal loss)
Proper lifetime (K^0_S)	<20 cm
Proper lifetime (Λ and $\bar{\Lambda}$)	<30 cm
K^0_S mass rejection window (Λ and $\bar{\Lambda}$)	± 10 MeV/c
Λ and $\bar{\Lambda}$ mass rejection window (K^0_S)	± 5 MeV/c

distribution subtracting the background from the peak region with a bin counting method. The background and signal regions are defined on the basis of the mass resolution as the windows in $[-12\sigma, -6\sigma]$, $[6\sigma, 12\sigma]$ and $[-6\sigma, 6\sigma]$, respectively. The value of σ changes with p_T to account for the actual mass resolution and ranges from about 3 MeV/c^2 to 7 MeV/c^2 for K^0_S and from about 1.4 MeV/c^2 to 2.5 MeV/c^2 for $\Lambda(\bar{\Lambda})$. More details on V^0 reconstruction can be found in [26,38]. The contribution from weak decays of the charged and neutral Ξ to the $\Lambda(\bar{\Lambda})$ yield has been corrected following a data-driven approach. The measured $\Xi^-(\bar{\Xi}^+)$ spectrum is used as input in a simulation of the decay kinematics to evaluate the fraction of reconstructed $\Lambda(\bar{\Lambda})$ coming from $\Xi^-(\bar{\Xi}^+)$ decays. The contribution from the decays of Ξ^0 is taken into account in the same way by assuming the ratio $\Xi^-(\bar{\Xi}^+)/\Xi^0 = 1$, as supported by statistical models and Pythia or DMPJET Monte Carlo simulations [40,41]. The raw transverse momentum distributions have been corrected for acceptance and reconstruction efficiency using a Monte Carlo simulation, based on the DPMJET 3.05 event generator [40] and a GEANT3.21 [42] model of the detector. As compared to the version used in [9,10], GEANT3.21 was improved by implementing a more realistic parameterization of the anti-proton inelastic cross-section [43]. A correction factor based on FLUKA [44] estimates was applied to negative kaons as in [9,10].

The study of systematic uncertainties follows the analysis described in [9,10] for $\pi^\pm$, $K^\pm$ and p($\bar{p}$). The main sources are the correction for secondary particles (4% for protons, 1% for pions, negligible for kaons), knowledge of the material budget (3% related to energy loss), hadronic interactions with the detector material (from 1% to 6%, more important at low p_T and for protons), tracking efficiency (4%), TOF matching efficiency (from 3 to 6%, depending on the particle) and PID (from 2% to 25%, depending on the particle and the p_T range). For the neutral Λ and K^0_S particles, the main sources are the level of knowledge of detector materials (resulting in a 4% uncertainty), track selections (up to 5%) and the feed-down correction for the Λ and $\bar{\Lambda}$ (5%), while topological selections contribute 2–4% depending on transverse momentum. The main sources of systematic uncertainties for the analysis of charged and neutral particles are summarized in Tables 3 and 4, respectively. The study of systematic uncertainties was repeated for the different multiplicity bins in order to separate the sources of uncertainty which are dependent on multiplicity and uncorrelated across different bins (depicted as shaded boxes in the figures).

3. Results

The p_T distributions of $\pi^\pm$, $K^\pm$, K^0_S, p($\bar{p}$) and $\Lambda(\bar{\Lambda})$ in $0 < y_{CMS} < 0.5$ are shown in Fig. 1 for different multiplicity intervals, as defined in Table 1. Particle/antiparticle as well as charged/neutral kaon transverse momentum distributions are identical within systematic uncertainties.

The p_T distributions show a clear evolution, becoming harder as the multiplicity increases. The change is most pronounced for

Table 3

Main sources of systematic uncertainty for $\pi^{\pm}$, $K^{\pm}$, p($\bar{p}$).

	$\pi^{\pm}$		$K^{\pm}$		p($\bar{p}$)	
p_T (GeV/c)	0.1	3	0.2	2.5	0.3	4
Correction for secondaries	1%	1%	negl.		4%	1%
Material budget	5%	negl.	2.5%	negl.	4%	negl.
Hadronic interactions	2%	1%	3%	1%	6%	1% ($\bar{p}$)
					4%	negl. (p)
Global tracking efficiency	4%		4%		4%	
Multiplicity dependence	2%	negl.	4%	negl.	2%	negl.
p_T (GeV/c)	0.1	0.6	0.2	0.5	0.3	0.6
ITS standalone tracking efficiency	5%	4%	6%	4.5%	6%	4.5%
ITS PID	1%		2%		1.5%	
p_T (GeV/c)	0.3	0.65	0.3	0.6	0.5	0.9
TPC PID	1.5%		3.5%		2.5%	
p_T (GeV/c)	0.5	3	0.5	2.5	0.5	4
TOF matching efficiency	4%	3%	5%	4%	5%	3%
TOF PID	1%	10%	2%	17%	2%	20%
p_T (GeV/c)	0.1	3	0.2	2.5	0.3	4
Total	7.5%	12%	8.5%	20%	9.5%	20%

Table 4

Main sources of systematic uncertainty for the K_S^0 and $\Lambda(\bar{\Lambda})$.

	K_S^0	$\Lambda(\bar{\Lambda})$	
Proper lifetime	2%	2%	
Material budget	4%	4%	
Track selection	4%	4%	
TPC PID	1%	1%	
Multiplicity dependence	2%	2%	
p_T (GeV/c)		<3.7	>3.7
Feed-down correction		5%	7%
p_T (GeV/c)		<3.7	>3.7
Total	6.5%	8%	9.5%

protons and lambdas. They show an increase of the slope at low p_T, similar to the one observed in heavy-ion collisions [9, 10]. The stronger multiplicity dependence of the spectral shapes of heavier particles is evident when looking at the ratios $K/\pi = (K^+ + K^-)/(\pi^+ + \pi^-)$, $p/\pi = (p + \bar{p})/(\pi^+ + \pi^-)$ and Λ/K_S^0 as functions of p_T, shown in Fig. 2 for the 0–5% and 60–80% event classes. The ratios p/π and Λ/K_S^0 show a significant enhancement at intermediate $p_T \sim 3$ GeV/c, qualitatively reminiscent of that measured in Pb–Pb collisions [9,10,38]. The latter are generally discussed in terms of collective flow or quark recombination [45–47]. However, the magnitude of the observed effects differs significantly between p–Pb and in Pb–Pb. The maximum of the p/π (Λ/K_S^0) ratio reaches $\sim$0.8 (1.5) in central Pb–Pb collisions, but only 0.4 (0.8) in the highest multiplicity p–Pb events. The highest multiplicity bin in p–Pb collisions exhibits ratios of p/π and Λ/K_S^0 which have maxima close to the corresponding ratios in the 60–70% bin in Pb–Pb collisions but differ somewhat in shape at lower p_T. The value of $dN_{ch}/d\eta$ in central p–Pb collisions (45±1) is a factor $\sim$1.7 lower than the one in the 60–70% Pb–Pb bin. A similar enhancement of the p/π ratio in high multiplicity d–Au collisions has also been reported for RHIC energies [48].

It is worth noticing that the ratio p/π as a function of $dN_{ch}/d\eta$ in a given p_T-bin follows a power-law behavior: $\frac{p}{\pi}(p_T) = A(p_T) \times [dN_{ch}/d\eta]^{B(p_T)}$. As shown in Fig. 3 (top), the same trend is also observed in Pb–Pb collisions. The exponent of the power-law function exhibits the same value in both collision systems (Fig. 3, middle). The same feature is also observed in the Λ/K_S^0 ratio (Fig. 3, bottom).

The p_T-integrated yields and $\langle p_T \rangle$ are computed using the data in the measured range and extrapolating them down to zero and to high p_T (up to 10 GeV/c). The fraction of extrapolated yield for high (low) multiplicity events is about 8% (9%), 10% (12%), 7% (13%), 17% (30%) for $\pi^{\pm}$, $K^{\pm}$, p and $\bar{p}$, Λ and $\bar{\Lambda}$ respectively and is negligible for K_S^0. Several parameterizations have been tested, among which the blast-wave function [11] (see below) gives the best description of the data over the full p_T range (Fig. 1). Other fit functions [49] (Boltzmann, m_T-exponential, p_T-exponential, Tsallis–Levy, Fermi–Dirac, Bose–Einstein) have been used to estimate the systematic uncertainty on the extrapolation, restricting the range to low p_T for those functions not giving a satisfactory description of the data over the full range. The uncertainty on the extrapolation amounts to about 2% for $\pi^{\pm}$, $K^{\pm}$, p($\bar{p}$), 3% (8% in low multiplicity events) for $\Lambda(\bar{\Lambda})$, and it is negligible for K_S^0 (since the p_T coverage ranges down to 0).

The $\langle p_T \rangle$ increases with multiplicity, at a rate which is stronger for heavier particles, as shown in Fig. 4. A similar mass ordering is also observed in pp [28] and Pb–Pb [10] collisions as a function of multiplicity.

In Fig. 5, the ratios to the pion yields are compared to Pb–Pb results at the LHC and Au–Au and d–Au results at RHIC [48–53]. While the p/π ratio shows no evolution from peripheral to central events, a small increase is observed in the K/π and Λ/π ratios, accounting for the bin-to-bin correlations of the uncertainties. A similar rise is observed in Pb–Pb, Au–Au and d–Au collisions. This is typically attributed to a reduced canonical suppression of strangeness production in larger freeze-out volumes [54] or to an enhanced strangeness production in a quark–gluon plasma [55].

The observations reported here are not strongly dependent on the actual variable used to select multiplicity classes. Alternative approaches, such as using the total charge in both VZERO-A and VZERO-C detectors, the energy deposited in the ZNA (which originates from neutrons of the Pb nucleus) and the number of clusters in the first ITS layers reveal very similar trends. In the cases where the largest deviation is observed, the p/π ratio is essentially the same in 0–5% events and it is $\sim$15% higher at $p_T \sim 3$ GeV/c in the 60–80% class. Part of this difference is due to the mild correlation of events at forward and central rapidity: the lowest multiplicity class selected with ZNA leads to a larger multiplicity at midrapidity than the corresponding class selected with the VZERO-A.
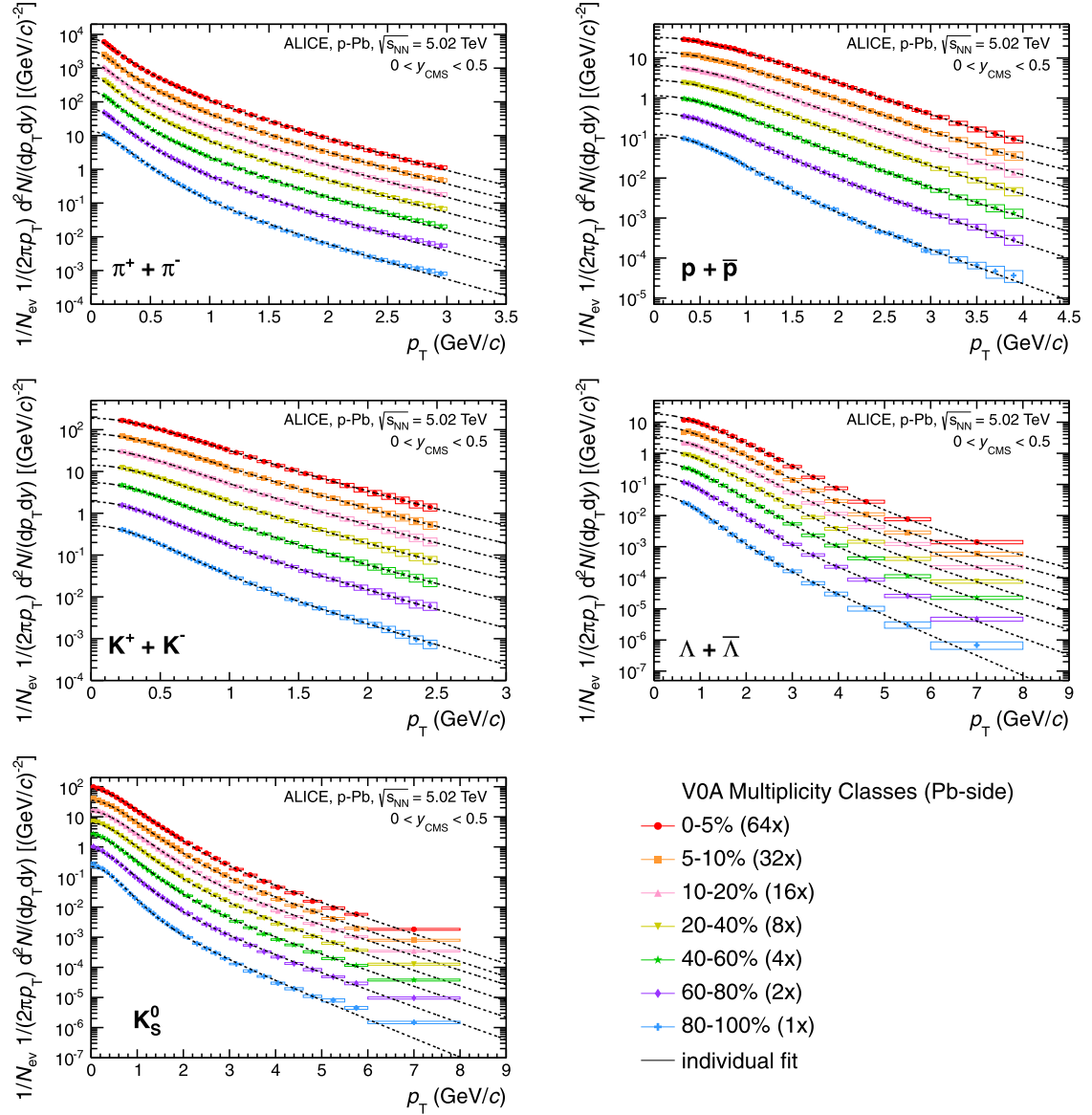
Fig. 1. (Color online.) Invariant p_T-differential yields of $\pi^\pm$, $K^\pm$, K_S^0, $p(\bar{p})$ and $\Lambda(\bar{\Lambda})$ in different V0A multiplicity classes (sum of particle and antiparticle states where relevant) measured in the rapidity interval $0 < y_{CMS} < 0.5$. Top to bottom: central to peripheral; data scaled by 2^n factors for better visibility. Statistical (bars) and full systematic (boxes) uncertainties are plotted. Dashed curves: blast-wave fits to each individual distribution.

4. Discussion

In heavy-ion collisions, the flattening of transverse momentum distribution and its mass ordering find their natural explanation in the collective radial expansion of the system [56]. This picture can be tested in a blast-wave framework with a simultaneous fit to all particles for each multiplicity bin. This parameterization assumes a locally thermalized medium, expanding collectively with a common velocity field and undergoing an instantaneous common freeze-out. The blast-wave functional form is given by [11]

$$\frac{1}{p_T}\frac{dN}{dp_T} \propto \int_0^R r\,dr\,m_T I_0\left(\frac{p_T \sinh\rho}{T_{kin}}\right) K_1\left(\frac{m_T \cosh\rho}{T_{kin}}\right), \tag{1}$$

where the velocity profile ρ is described by

$$\rho = \tanh^{-1}\beta_T = \tanh^{-1}\left(\left(\frac{r}{R}\right)^n \beta_s\right). \tag{2}$$

Here, $m_T = \sqrt{p_T^2 + m^2}$ is the transverse mass, I_0 and K_1 are the modified Bessel functions, r is the radial distance from the center of the fireball in the transverse plane, R is the radius of the fireball, $\beta_T(r)$ is the transverse expansion velocity, β_s is the transverse expansion velocity at the surface, n is the exponent of the velocity profile and T_{kin} is the kinetic freeze-out temperature. The free parameters in the fit are T_{kin}, β_s, n and a normalization parameter.

In contrast with the individual fits discussed above, the simultaneous fit to all particle species under consideration can provide insight on the (common) kinetic freeze-out properties of the system. It has to be kept in mind, however, that the actual values of the fit parameters depend substantially on the fit range [10]. In spite of this limitations, the blast-wave model still provides a handy way to compare the transverse momentum distributions and their evolution in different collision systems.

The fit presented in this Letter is performed in the same range as in [9,10], also including K_S^0 and $\Lambda(\bar{\Lambda})$. The ranges 0.5–1 GeV/c,
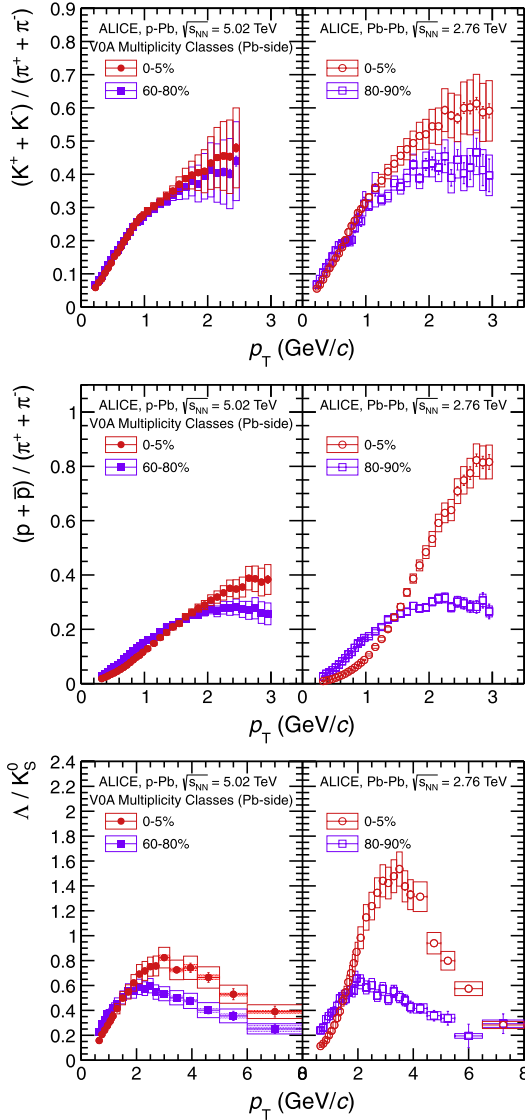
Fig. 2. (Color online.) Ratios $K/\pi = (K^+ + K^-)/(\pi^+ + \pi^-)$, $p/\pi = (p+\bar{p})/(\pi^+ + \pi^-)$ and Λ/K_S^0 as a function of p_T in two multiplicity bins measured in the rapidity interval $0 < y_{CMS} < 0.5$ (left panels). The ratios are compared to results in Pb–Pb collisions measured at mid-rapidity, shown in the right panels. The empty boxes show the total systematic uncertainty; the shaded boxes indicate the contribution uncorrelated across multiplicity bins (not estimated in Pb–Pb).

Fig. 3. (Color online.) p/π ratio as a function of the charged-particle density $dN_{ch}/d\eta$ in three p_T intervals in p–Pb (measured in the rapidity interval $0 < y_{CMS} < 0.5$) and Pb–Pb collisions (measured at mid-rapidity). The dashed lines show the corresponding power-law fit (top). Exponent of the p/π (middle) and Λ/K_S^0 (bottom) power-law fit as a function of p_T in p–Pb and Pb–Pb collisions. The empty boxes show the total systematic uncertainty; the shaded boxes indicate the contribution uncorrelated across multiplicity bins (not estimated in Pb–Pb).

0.2–1.5 GeV/c, 0–1.5 GeV/c, 0.3–3 GeV/c and 0.6–3 GeV/c have been used for $\pi^\pm$, $K^\pm$, K_S^0, p($\bar{p}$) and $\Lambda(\bar{\Lambda})$ respectively. They have been defined according to the available data at low p_T and based on the agreement with the data at high p_T, justified considering that the assumptions underlying the blast-wave model are not expected to be valid at high p_T. Excluding the K_S^0 and $\Lambda(\bar{\Lambda})$ from the fit causes a negligible difference in the fit parameters.

The results are reported in Table 5 and Fig. 6. Variations of the fit range lead to large shifts (∼10%) of the fit results (correlated across centralities), as discussed for Pb–Pb data in [9,10].

As can be seen in Fig. 6, the parameters show a similar trend as the ones obtained in Pb–Pb. Within the limitations of the blast-wave model, this observation is consistent with the presence of radial flow in p–Pb collisions. A detailed comparison of the resulting fit parameters between Pb–Pb [9,10] and p–Pb (Table 5) collisions shows that at similar $dN_{ch}/d\eta$ the values of parameters

for T_{kin} are similar for the two systems, whereas the $\langle\beta_T\rangle$ values are significantly higher in p–Pb collisions. While in Pb–Pb collisions high multiplicity events are obtained through multiple soft interactions, in p–Pb collisions the high multiplicity selection biases the sample towards harder collisions [57]. This could lead to the larger $\langle\beta_T\rangle$ parameter obtained from the blast-wave fits. Under the assumptions of a collective hydrodynamic expansion, a larger radial velocity in p–Pb collisions has been suggested as a consequence of stronger radial gradients in [58].

In a hydrodynamically expanding system, the flow coefficients v_n are also expected to exhibit a characteristic mass-dependent ordering depending on the transverse expansion velocity. To probe this picture, the p_T distributions are fitted simultaneously with the elliptic flow coefficient extracted from two particle correlations v_2 of $\pi^\pm$, $K^\pm$, p($\bar{p}$) measured in [59], with the extension of the
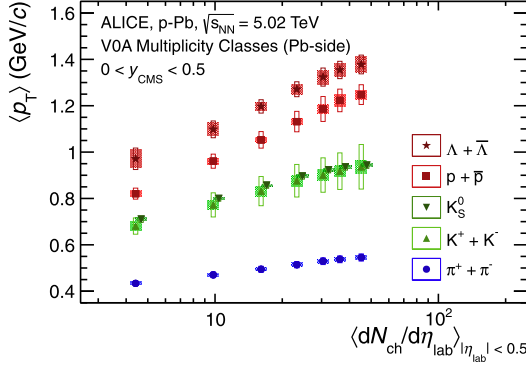
Fig. 4. (Color online.) Mean transverse momentum as a function of $dN_{ch}/d\eta$ in each V0A multiplicity class (see text for details) for different particle species. The $dN_{ch}/d\eta$ values of K_S^0 are shifted for visibility. The empty boxes show the total systematic uncertainty; the shaded boxes indicate the contribution uncorrelated across multiplicity bins.

blast-wave model of [60]. This global fit is found to describe the v_2 of pions, kaons and protons relatively well, even if the quality of the fit is slightly worse than that of similar fits in Pb–Pb collisions, in particular for the proton v_2. Compared to the case where only the particle p_T-differential yields are used, the fit results of T_{kin} and $\langle \beta_T \rangle$ differ by about 2% only.

Other processes not related to hydrodynamic collectivity could also be responsible for the observed results. This is illustrated in Fig. 6, which shows the results obtained by applying the same fitting procedure to transverse momentum distributions from the simulation of pp collisions at $\sqrt{s} = 7$ TeV with the PYTHIA8 event generator (tune 4C) [61], a model not including any collective system expansion. PYTHIA8 events are divided into several classes according to the charged-particle multiplicity at mid-rapidity $|\eta_{lab}| < 0.3$, namely $N_{ch} < 5$, $5 \leqslant N_{ch} < 10$, $10 \leqslant N_{ch} < 15$, $15 \leqslant N_{ch} < 20$ and $N_{ch} \geqslant 20$. The fit results are shown for PYTHIA8 simulations performed both with and without the color reconnection mechanism [62,63]. This mechanism is necessary in PYTHIA tunes to describe the evolution of $\langle p_T \rangle$ with multiplicity in pp collisions [57]. With color reconnection the evolution of PYTHIA8 transverse momentum distributions follows a similar trend as the one observed for p–Pb and Pb–Pb collisions at the LHC, while without color reconnection it is not as strong. This generator study shows that other final state mechanisms, such as color reconnection, can mimic the effects of radial flow [64].

The p_T distributions in the 5–10% bin are compared in Fig. 7 with calculations from the DPMJET, Kraków [65] and EPOS LHC 1.99 v3400 [66] models. The QCD-inspired DPMJET [40] generator, which is based on the Gribov–Glauber approach, treats soft and hard scattering processes in an unified way. It has been found to
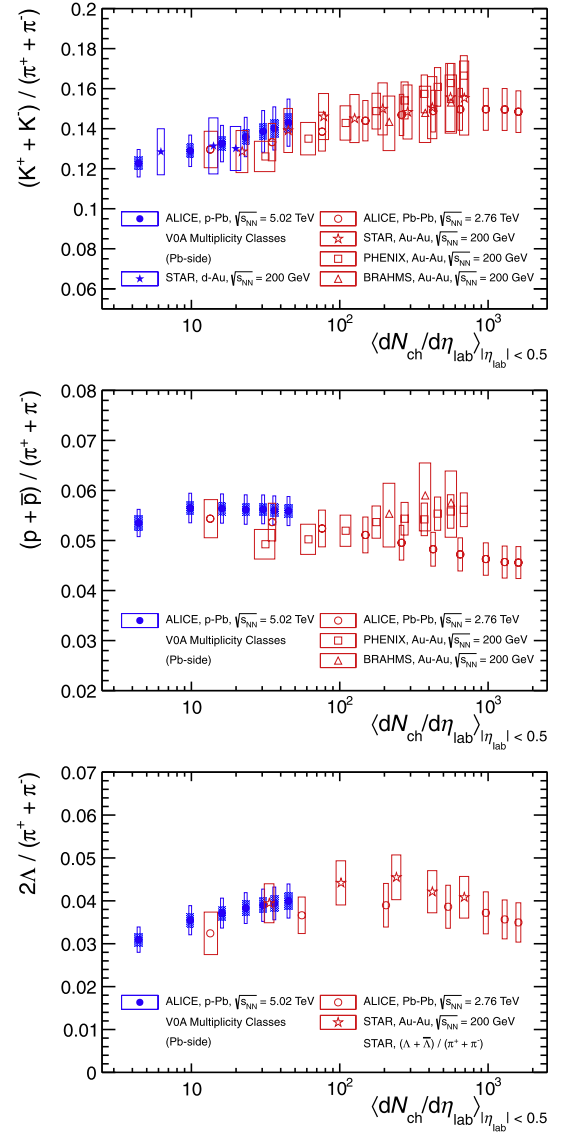

Fig. 5. (Color online.) Particle yields dN/dy of kaons, protons, and lambdas normalized to pions as a function of $dN_{ch}/d\eta$ in each V0A multiplicity class (see text for details) measured in the rapidity interval $0 < y_{CMS} < 0.5$. The values are compared to results obtained from Pb–Pb collisions at the LHC and Au–Au and d–Au collisions at RHIC measured at mid-rapidity. The empty boxes show the total systematic uncertainty; the shaded boxes indicate the contribution uncorrelated across multiplicity bins (not estimated in Pb–Pb).

successfully reproduce the pseudo-rapidity distribution of charged particles in NSD p–Pb collisions at the LHC as reported in [33]. On the other hand, it cannot reproduce the p_T distribution [67] and

Table 5
Blast-wave parameters for simultaneous p–Pb fit of $\pi^\pm$, $K^\pm$, K_S^0, $p(\bar{p})$ and $\Lambda(\bar{\Lambda})$ in the fit ranges 0.5–1 GeV/c, 0.2–1.5 GeV/c, 0–1.5 GeV/c, 0.3–3 GeV/c and 0.6–3 GeV/c, respectively. Positive and negative variations of the parameters using the different fit ranges as done in [9,10] are also reported.

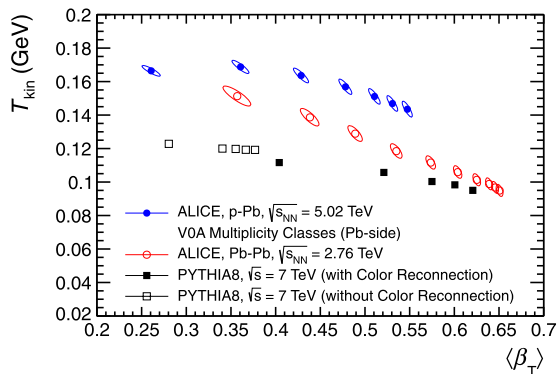| Event class	$\langle \beta_T \rangle$	T_{kin} (GeV/c)	n	χ^2/ndf
0–5%	$0.547 \pm 0.006^{+0.01}_{-0.02}$	$0.143 \pm 0.005^{+0.01}_{-0.01}$	$1.07 \pm 0.03^{+0.08}_{-0.09}$	0.27
5–10%	$0.531 \pm 0.006^{+0.01}_{-0.03}$	$0.147 \pm 0.005^{+0.01}_{-0.01}$	$1.14 \pm 0.03^{+0.1}_{-0.2}$	0.33
10–20%	$0.511 \pm 0.007^{+0.01}_{-0.03}$	$0.151 \pm 0.005^{+0.02}_{-0.01}$	$1.24 \pm 0.04^{+0.2}_{-0.2}$	0.36
20–40%	$0.478 \pm 0.007^{+0.02}_{-0.03}$	$0.157 \pm 0.005^{+0.02}_{-0.02}$	$1.41 \pm 0.05^{+0.2}_{-0.2}$	0.35
40–60%	$0.428 \pm 0.009^{+0.03}_{-0.03}$	$0.164 \pm 0.004^{+0.02}_{-0.02}$	$1.73 \pm 0.07^{+0.2}_{-0.4}$	0.43
60–80%	$0.36 \pm 0.01^{+0.04}_{-0.02}$	$0.169 \pm 0.004^{+0.02}_{-0.02}$	$2.4 \pm 0.1^{+0.2}_{-0.6}$	0.54
80–100%	$0.26 \pm 0.01^{+0.03}_{-0.01}$	$0.166 \pm 0.003^{+0.02}_{-0.01}$	$3.9 \pm 0.3^{+0.1}_{-0.7}$	0.84

Fig. 6. (Color online.) Results of blast-wave fits, compared to Pb–Pb data and MC simulations from PYTHIA8 with and without color reconnection. Charged-particle multiplicity increases from left to right. Uncertainties from the global fit are shown as correlation ellipses.
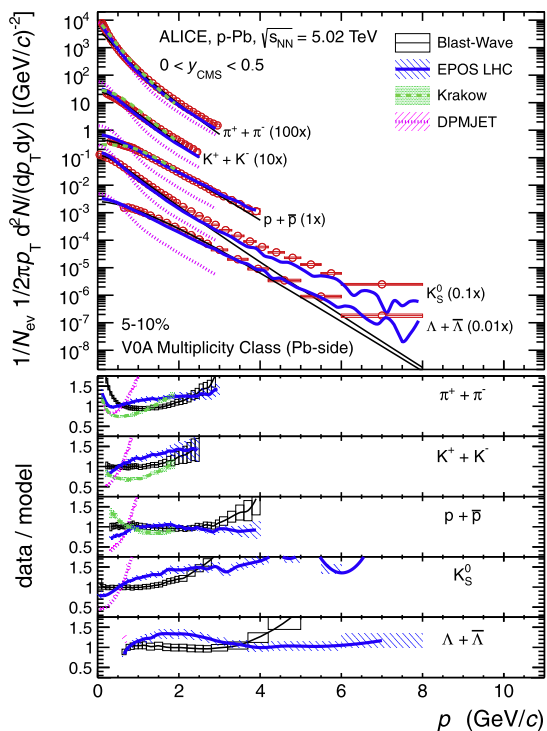

Fig. 7. (Color online.) Pion, kaon, and proton transverse momentum distributions in the 5–10% V0A multiplicity class measured in the rapidity interval $0 < y_{CMS} < 0.5$ compared to the several models (see text for details).

the $\langle p_T \rangle$ of charged particles [57]. In the Kraków hydrodynamic model, fluctuating initial conditions are implemented based on a Glauber model using a Monte Carlo simulation. The expansion of the system is calculated event-by-event in a $3 + 1$ dimensional viscous hydrodynamic approach and the freeze-out follows statistical hadronization in a Cooper–Frye formalism. In the EPOS model, founded on "parton-based Gribov Regge theory", the initial hard and soft scattering creates "flux tubes" which either escape the medium and hadronize as jets or contribute to the bulk matter, described in terms of hydrodynamics. The version of the model used here implements a simplified treatment of the collective expansion [66]. EPOS predictions including the full hydrodynamic calculation [68] are not available at the time of writing.

The transverse momentum distributions in the 5–10% multiplicity class are compared to the predictions by Kraków for $11 \leqslant N_{part} \leqslant 17$, since the $dN_{ch}/d\eta$ from the model matches best with the measured value in this class. DPMJET and EPOS events have been selected according to the charged-particle multiplicity in the VZERO-A acceptance in order to match the experimental selection. DPMJET distributions are softer than the measured ones and the model overpredicts the production of all particles for p_T lower than about 0.5–0.7 GeV/c and underpredicts it at higher momenta. At high p_T, the p_T spectra shapes of pions and kaons are rather well reproduced for momenta above 1 and 1.5 GeV/c respectively. Final state effects may be needed in order to reproduce the data. In fact, the Kraków model reproduces reasonably well the spectral shapes of pions and kaons below transverse momenta of 1 GeV/c where hydrodynamic effects are expected to dominate. For higher momenta, the observed deviations for pions and kaons could be explained in a hydrodynamic framework as due to the onset of a non-thermal component. EPOS can reproduce the pion and proton distributions within 20% over the full measured range, while larger deviations are seen for kaons and lambdas. The yield and the shape of the p_T distributions of protons are rather well described by both models. In contrast to a similar comparison for Pb–Pb collisions [9, 10], in the Kraków calculation the yield of pions and kaons seems to be overestimated. It is interesting to notice that when final state interactions are disabled in EPOS, the description of many pp and p–Pb observables worsens significantly [66].

5. Conclusions

In summary, we presented a comprehensive measurement of $\pi^{\pm}$, $K^{\pm}$, K_S^0, $p(\bar{p})$ and $\Lambda(\bar{\Lambda})$ in p–Pb collisions at $\sqrt{s_{NN}} = 5.02$ TeV at the LHC. These data represent a crucial set of constraints for the modeling of proton–lead collisions at the LHC. The transverse momentum distributions show a clear evolution with multiplicity, similar to the pattern observed in high-energy pp and heavy-ion collisions, where in the latter case the effect is usually attributed to collective radial expansion. Models incorporating final state effects give a better description of the data.

References

[1] N. Cabibbo, G. Parisi, Exponential hadronic spectrum and quark liberation, Phys. Lett. B 59 (1975) 67–69.

[2] E.V. Shuryak, Quark–gluon plasma and hadronic production of leptons, photons and psions, Phys. Lett. B 78 (1978) 150.

[3] L.D. McLerran, B. Svetitsky, A Monte Carlo study of SU(2) Yang–Mills theory at finite temperature, Phys. Lett. B 98 (1981) 195.

[4] E. Laermann, O. Philipsen, The status of lattice QCD at finite temperature, Annu. Rev. Nucl. Part. Sci. 53 (2003) 163–198.

[5] B. Muller, J.L. Nagle, Results from the relativistic heavy ion collider, Annu. Rev. Nucl. Part. Sci. 56 (2006) 93–135.

[6] A. Andronic, P. Braun-Munzinger, J. Stachel, Thermal hadron production in relativistic nuclear collisions: the hadron mass spectrum, the horn, and the QCD phase transition, Phys. Lett. B 673 (2009) 142–145.

[7] J. Cleymans, I. Kraus, H. Oeschler, K. Redlich, S. Wheaton, Statistical model predictions for particle ratios at $\sqrt{s_{NN}} = 5.5$ TeV, Phys. Rev. C 74 (2006) 034903.

[8] P. Braun-Munzinger, J. Stachel, C. Wetterich, Chemical freeze-out and the QCD phase transition temperature, Phys. Lett. B 596 (2004) 61–69.

[9] ALICE Collaboration, B. Abelev, et al., Pion, kaon, and proton production in central Pb–Pb collisions at $\sqrt{s_{NN}} = 2.76$ TeV, Phys. Rev. Lett. 109 (2012) 252301.

[10] ALICE Collaboration, B. Abelev, et al., Centrality dependence of π, K, p production in Pb–Pb collisions at $\sqrt{s_{NN}} = 2.76$ TeV, arXiv:1303.0737 [hep-ex].

[11] E. Schnedermann, J. Sollfrank, U.W. Heinz, Thermal phenomenology of hadrons from 200 A/GeV S + S collisions, Phys. Rev. C 48 (1993) 2462–2475.

[12] PHOBOS Collaboration, B. Alver, et al., Phobos results on charged particle multiplicity and pseudorapidity distributions in Au + Au, Cu + Cu, d + Au, and p + p collisions at ultra-relativistic energies, Phys. Rev. C 83 (2011) 024913, arXiv:1011.1940 [nucl-ex].

[13] L.D. McLerran, R. Venugopalan, Computing quark and gluon distribution functions for very large nuclei, Phys. Rev. D 49 (1994) 2233–2241.

[14] F. Gelis, E. Iancu, J. Jalilian-Marian, R. Venugopalan, The color glass condensate, Annu. Rev. Nucl. Part. Sci. 60 (2010) 463–489.

[15] CMS Collaboration, V. Khachatryan, et al., Observation of long-range near-side angular correlations in proton–proton collisions at the LHC, J. High Energy Phys. 1009 (2010) 091.

[16] CMS Collaboration, S. Chatrchyan, et al., Observation of long-range near-side angular correlations in proton–lead collisions at the LHC, Phys. Lett. B 718 (2013) 795–814.

[17] ALICE Collaboration, B. Abelev, et al., Long-range angular correlations on the near and away side in p–Pb collisions at $\sqrt{s_{NN}} = 5.02$ TeV, Phys. Lett. B 719 (2012) 29–41.

[18] ATLAS Collaboration, G. Aad, et al., Observation of associated near-side and away-side long-range correlations in $\sqrt{s_{NN}} = 5.02$ TeV proton–lead collisions with the ATLAS detector, arXiv:1212.5198 [hep-ex].

[19] ATLAS Collaboration, G. Aad, et al., Measurement with the ATLAS detector of multi-particle azimuthal correlations in p + Pb collisions at $\sqrt{s_{NN}} = 5.02$ TeV, Phys. Lett. B 725 (2013) 60–78, arXiv:1303.2084 [hep-ex].

[20] CMS Collaboration, S. Chatrchyan, et al., Multiplicity and transverse momentum dependence of two- and four-particle correlations in p–Pb and Pb–Pb collisions, Phys. Lett. B 724 (2013) 213–240, arXiv:1305.0609 [nucl-ex].

[21] K. Dusling, R. Venugopalan, Comparison of the color glass condensate to di-hadron correlations in proton–proton and proton–nucleus collisions, Phys. Rev. D 87 (2013), 094034.

[22] P. Bozek, W. Broniowski, Correlations from hydrodynamic flow in p–Pb collisions, Phys. Lett. B 718 (2013) 1557–1561.

[23] G.-Y. Qin, B. Müller, Elliptic and triangular flow anisotropy in deuteron–gold collisions at RHIC and proton–lead collisions at the LHC, arXiv:1306.3439 [nucl-th].

[24] A. Bzdak, B. Schenke, P. Tribedy, R. Venugopalan, Initial state geometry and the role of hydrodynamics in proton–proton, proton–nucleus and deuteron–nucleus collisions, arXiv:1304.3403 [nucl-th].

[25] ALICE Collaboration, K. Aamodt, et al., Production of pions, kaons and protons in pp collisions at $\sqrt{s} = 900$ GeV with ALICE at the LHC, Eur. Phys. J. C 71 (2011) 1655.

[26] ALICE Collaboration, K. Aamodt, et al., Strange particle production in proton–proton collisions at $\sqrt{s} = 0.9$ TeV with ALICE at the LHC, Eur. Phys. J. C 71 (2011) 1594.

[27] ALICE Collaboration, B. Abelev, et al., Multi-strange baryon production in pp collisions at $\sqrt{s} = 7$ TeV with ALICE, Phys. Lett. B 712 (2012) 309–318.

[28] CMS Collaboration, S. Chatrchyan, et al., Study of the inclusive production of charged pions, kaons, and protons in pp collisions at $\sqrt{s} = 0.9, 2.76$, and 7 TeV, Eur. Phys. J. C 72 (2012) 2164.

[29] CMS Collaboration, V. Khachatryan, et al., Strange particle production in pp collisions at $\sqrt{s_{NN}} = 0.9$ and 7 TeV, J. High Energy Phys. 1105 (2011) 064.

[30] CMS Collaboration, S. Chatrchyan, et al., Study of the production of charged pions, kaons, and protons in p–Pb collisions at $\sqrt{s_{NN}} = 5.02$ TeV, arXiv:1307.3442 [hep-ex].

[31] L. Evans, P. Bryant, LHC machine, J. Instrum. 3 (2008), S08001.

[32] ALICE Collaboration, K. Aamodt, et al., The ALICE experiment at the CERN LHC, J. Instrum. 3 (2008), S08002.

[33] ALICE Collaboration, B. Abelev, et al., Pseudorapidity density of charged particles p–Pb collisions at $\sqrt{s_{NN}} = 5.02$ TeV, Phys. Rev. Lett. 110 (2013) 032301.

[34] ALICE Collaboration, K. Aamodt, et al., Charged-particle multiplicity measurement in proton–proton collisions at $\sqrt{s} = 7$ TeV with ALICE at LHC, Eur. Phys. J. C 68 (2010) 345–354.

[35] J. Alme, Y. Andres, H. Appelshauser, S. Bablok, N. Bialas, et al., The ALICE TPC, a large 3-dimensional tracking device with fast readout for ultra-high multiplicity events, Nucl. Instrum. Methods Phys. Res., Sect. A, Accel. Spectrom. Detect. Assoc. Equip. 622 (2010) 316–367.

[36] A. Akindinov, A. Alici, A. Agostinelli, P. Antonioli, S. Arcelli, et al., Performance of the ALICE time-of-flight detector at the LHC, Eur. Phys. J. Plus 128 (2013) 44.

[37] ALICE Collaboration, Performance of the ALICE Experiment at CERN LHC, in preparation.

[38] ALICE Collaboration, K$_S^0$ and Λ production in Pb–Pb collisions at $\sqrt{s_{NN}} = 2.76$ TeV, arXiv:1307.5530 [nucl-ex].

[39] Particle Data Group, J. Beringer, et al., Review of Particle Physics (RPP), Phys. Rev. D 86 (2012), 010001.

[40] S. Roesler, R. Engel, J. Ranft, The Monte Carlo event generator DPMJET-III, arXiv:hep-ph/0012252.

[41] P.Z. Skands, Tuning Monte Carlo generators: the Perugia tunes, Phys. Rev. D 82 (2010), 074018.

[42] R. Brun, F. Carminati, S. Giani, GEANT detector description and simulation tool, CERN-W5013, CERN-W-5013.

[43] A.A. Moiseev, J.F. Ormes, Inelastic cross section for antihelium on nuclei: an empirical formula for use in the experiments to search for cosmic antimatter, Astropart. Phys. 6 (1997) 379–386.

[44] G. Battistoni, S. Muraro, P.R. Sala, F. Cerutti, A. Ferrari, et al., The FLUKA code: description and benchmarking, AIP Conf. Proc. 896 (2007) 31–49.

[45] R. Fries, B. Muller, C. Nonaka, S. Bass, Hadronization in heavy ion collisions: recombination and fragmentation of partons, Phys. Rev. Lett. 90 (2003) 202303.

[46] P. Bozek, Hydrodynamic flow from RHIC to LHC, arXiv:1111.4398 [nucl-th].

[47] B. Muller, J. Schukraft, B. Wyslouch, First results from Pb + Pb collisions at the LHC, Annu. Rev. Nucl. Part. Sci. 62 (2012) 361–386.

[48] PHENIX Collaboration, A. Adare, et al., Spectra and ratios of identified particles in Au + Au and d + Au collisions at $\sqrt{s_{NN}} = 200$ GeV, Phys. Rev. C 88 (2013), 024906.

[49] STAR Collaboration, B. Abelev, et al., Systematic measurements of identified particle spectra in pp, d + Au and Au + Au collisions from STAR, Phys. Rev. C 79 (2009) 034909.

[50] STAR Collaboration, G. Agakishiev, et al., Strangeness enhancement in Cu + Cu and Au + Au collisions at $\sqrt{s_{NN}} = 200$ GeV, Phys. Rev. Lett. 108 (2012) 072301.

[51] STAR Collaboration, M. Aggarwal, et al., Strange and multi-strange particle production in Au + Au collisions at $\sqrt{s_{NN}}$ = 62.4 GeV, Phys. Rev. C 83 (2011) 024901.

[52] PHENIX Collaboration, S.S. Adler, et al., Identified charged particle spectra and yields in Au + Au collisions at $\sqrt{s_{NN}}$ = 200 GeV, Phys. Rev. C 69 (2004) 034909.

[53] BRAHMS Collaboration, I. Arsene, et al., Centrality dependent particle production at $y = 0$ and $y \sim 1$ in Au + Au collisions at $\sqrt{s_{NN}}$ = 200 GeV, Phys. Rev. C 72 (2005) 014908.

[54] J. Sollfrank, F. Becattini, K. Redlich, H. Satz, Canonical strangeness enhancement, Nucl. Phys. A 638 (1998) 399C–402C.

[55] J. Letessier, J. Rafelski, Strangeness chemical equilibration in QGP at RHIC and CERN LHC, Phys. Rev. C 75 (2007) 014905.

[56] U.W. Heinz, Concepts of heavy ion physics, CERN-2004-001-D, 2004.

[57] ALICE Collaboration, B. Abelev, et al., Multiplicity dependence of the average transverse momentum in pp, p–Pb, and Pb–Pb collisions at the LHC, arXiv:1307.1094 [nucl-ex].

[58] E. Shuryak, I. Zahed, High multiplicity pp and pA collisions: hydrodynamics at its edge and stringy black hole, arXiv:1301.4470 [hep-ph].

[59] ALICE Collaboration, B. Abelev, et al., Long-range angular correlations of π, K and p in p–Pb collisions at $\sqrt{s_{NN}}$ = 5.02 TeV, arXiv:1307.3237 [nucl-ex].

[60] P. Huovinen, P. Kolb, U.W. Heinz, P. Ruuskanen, S. Voloshin, Radial and elliptic flow at RHIC: further predictions, Phys. Lett. B 503 (2001) 58–64.

[61] R. Corke, T. Sjostrand, Interleaved parton showers and tuning prospects, J. High Energy Phys. 1103 (2011) 032.

[62] P.Z. Skands, D. Wicke, Non-perturbative QCD effects and the top mass at the Tevatron, Eur. Phys. J. C 52 (2007) 133–140.

[63] H. Schulz, P. Skands, Energy scaling of minimum-bias tunes, Eur. Phys. J. C 71 (2011) 1644.

[64] A. Ortiz, P. Christiansen, E. Cuautle, I. Maldonado, G. Paic, Color reconnection and flow-like patterns in pp collisions, Phys. Rev. Lett. 111 (2013) 042001.

[65] P. Bozek, Collective flow in p–Pb and d–Pd collisions at TeV energies, Phys. Rev. C 85 (2012) 014911.

[66] T. Pierog, I. Karpenko, J. Katzy, E. Yatsenko, K. Werner, EPOS LHC: test of collective hadronization with LHC data, arXiv:1306.0121 [hep-ph].

[67] ALICE Collaboration, B. Abelev, et al., Transverse momentum distribution and nuclear modification factor of charged particles in p–Pb collisions at $\sqrt{s_{NN}}$ = 5.02 TeV, Phys. Rev. Lett. 110 (2012) 082302.

[68] K. Werner, I. Karpenko, M. Bleicher, T. Pierog, S. Porteboeuf-Houssais, Jets, bulk matter, and their interaction in heavy ion collisions at several TeV, Phys. Rev. C 85 (2012) 064907.

ALICE Collaboration

B. Abelev [bq], J. Adam [aj], D. Adamová [by], A.M. Adare [dv], M.M. Aggarwal [cc], G. Aglieri Rinella [ag], M. Agnello [ci,cz], A.G. Agocs [du], A. Agostinelli [y], Z. Ahammed [dq], N. Ahmad [p], A. Ahmad Masoodi [p], I. Ahmed [n], S.U. Ahn [bj], S.A. Ahn [bj], I. Aimo [cz,ci], S. Aiola [dv], M. Ajaz [n], A. Akindinov [ba], D. Aleksandrov [co], B. Alessandro [cz], D. Alexandre [cq], A. Alici [k,ct], A. Alkin [c], J. Alme [ah], T. Alt [al], V. Altini [ad], S. Altinpinar [q], I. Altsybeev [dp], C. Alves Garcia Prado [dg], C. Andrei [bt], A. Andronic [cl], V. Anguelov [ch], J. Anielski [av], T. Antičić [cm], F. Antinori [cw], P. Antonioli [ct], L. Aphecetche [da], H. Appelshäuser [at], N. Arbor [bm], S. Arcelli [y], N. Armesto [o], R. Arnaldi [cz], T. Aronsson [dv], I.C. Arsene [cl], M. Arslandok [at], A. Augustinus [ag], R. Averbeck [cl], T.C. Awes [bz], M.D. Azmi [ce], M. Bach [al], A. Badalà [cv], Y.W. Baek [bl,am], R. Bailhache [at], V. Bairathi [cg], R. Bala [cz,cf], A. Baldisseri [m], F. Baltasar Dos Santos Pedrosa [ag], J. Bán [bb], R.C. Baral [bd], R. Barbera [z], F. Barile [ad], G.G. Barnaföldi [du], L.S. Barnby [cq], V. Barret [bl], J. Bartke [dd], M. Basile [y], N. Bastid [bl], S. Basu [dq], B. Bathen [av], G. Batigne [da], B. Batyunya [bi], P.C. Batzing [t], C. Baumann [at], I.G. Bearden [bv], H. Beck [at], N.K. Behera [ap], I. Belikov [aw], F. Bellini [y], R. Bellwied [di], E. Belmont-Moreno [bg], G. Bencedi [du], S. Beole [w], I. Berceanu [bt], A. Bercuci [bt], Y. Berdnikov [ca], D. Berenyi [du], A.A.E. Bergognon [da], R.A. Bertens [az], D. Berzano [w], L. Betev [ag], A. Bhasin [cf], A.K. Bhati [cc], J. Bhom [dm], L. Bianchi [w], N. Bianchi [bn], J. Bielčík [aj], J. Bielčíková [by], A. Bilandzic [bv], S. Bjelogrlic [az], F. Blanco [i], F. Blanco [di], D. Blau [co], C. Blume [at], F. Bock [bp,ch], A. Bogdanov [br], H. Bøggild [bv], M. Bogolyubsky [ax], L. Boldizsár [du], M. Bombara [ak], J. Book [at], H. Borel [m], A. Borissov [dt], J. Bornschein [al], M. Botje [bw], E. Botta [w], S. Böttger [as], P. Braun-Munzinger [cl], M. Bregant [da], T. Breitner [as], T.A. Broker [at], T.A. Browning [cj], M. Broz [ai], R. Brun [ag], E. Bruna [cz], G.E. Bruno [ad], D. Budnikov [cn], H. Buesching [at], S. Bufalino [cz], P. Buncic [ag], O. Busch [ch], Z. Buthelezi [bh], D. Caffarri [aa], X. Cai [f], H. Caines [dv], A. Caliva [az], E. Calvo Villar [cr], P. Camerini [v], V. Canoa Roman [j,ag], G. Cara Romeo [ct], F. Carena [ag], W. Carena [ag], F. Carminati [ag], A. Casanova Díaz [bn], J. Castillo Castellanos [m], E.A.R. Casula [u], V. Catanescu [bt], C. Cavicchioli [ag], C. Ceballos Sanchez [h], J. Cepila [aj], P. Cerello [cz], B. Chang [dj], S. Chapeland [ag], J.L. Charvet [m], S. Chattopadhyay [dq], S. Chattopadhyay [cp], M. Cherney [cb], C. Cheshkov [do], B. Cheynis [do], V. Chibante Barroso [ag], D.D. Chinellato [di], P. Chochula [ag], M. Chojnacki [bv], S. Choudhury [dq], P. Christakoglou [bw], C.H. Christensen [bv], P. Christiansen [ae], T. Chujo [dm], S.U. Chung [ck], C. Cicalo [cu], L. Cifarelli [k,y], F. Cindolo [ct], J. Cleymans [ce], F. Colamaria [ad], D. Colella [ad], A. Collu [u], M. Colocci [y], G. Conesa Balbastre [bm], Z. Conesa del Valle [ar,ag], M.E. Connors [dv], G. Contin [v], J.G. Contreras [j], T.M. Cormier [dt], Y. Corrales Morales [w], P. Cortese [ac], I. Cortés Maldonado [b], M.R. Cosentino [bp], F. Costa [ag], P. Crochet [bl], R. Cruz Albino [j], E. Cuautle [bf], L. Cunqueiro [bn,ag], A. Dainese [cw], R. Dang [f], A. Danu [be], K. Das [cp], D. Das [cp], I. Das [ar], A. Dash [dh], S. Dash [ap], S. De [dq], H. Delagrange [da], E. Dénes [du], A. Deppman [dg], G.O.V. de Barros [dg], A. De Caro [k,ab], G. de Cataldo [cs], J. de Cuveland [al], A. De Falco [u], D. De Gruttola [ab,k], N. De Marco [cz], S. De Pasquale [ab], R. de Rooij [az], M.A. Diaz Corchero [i], T. Dietel [av], R. Divià [ag], D. Di Bari [ad], C. Di Giglio [ad], S. Di Liberto [cx], A. Di Mauro [ag], P. Di Nezza [bn], Ø. Djuvsland [q], A. Dobrin [az,dt], T. Dobrowolski [bs], B. Dönigus [cl,at], O. Dordic [t], A.K. Dubey [dq], A. Dubla [az], L. Ducroux [do], P. Dupieux [bl], A.K. Dutta Majumdar [cp], G. D Erasmo [ad], D. Elia [cs], D. Emschermann [av], H. Engel [as],

B. Erazmus [ag,da], H.A. Erdal [ah], D. Eschweiler [al], B. Espagnon [ar], M. Estienne [da], S. Esumi [dm], D. Evans [cq],
S. Evdokimov [ax], G. Eyyubova [t], D. Fabris [cw], J. Faivre [bm], D. Falchieri [y], A. Fantoni [bn], M. Fasel [ch],
D. Fehlker [q], L. Feldkamp [av], D. Felea [be], A. Feliciello [cz], G. Feofilov [dp], J. Ferencei [by], A. Fernández Téllez [b],
E.G. Ferreiro [o], A. Ferretti [w], A. Festanti [aa], J. Figiel [dd], M.A.S. Figueredo [dg], S. Filchagin [cn], D. Finogeev [ay],
F.M. Fionda [ad], E.M. Fiore [ad], E. Floratos [cd], M. Floris [ag], S. Foertsch [bh], P. Foka [cl], S. Fokin [co],
E. Fragiacomo [cy], A. Francescon [aa,ag], U. Frankenfeld [cl], U. Fuchs [ag], C. Furget [bm], M. Fusco Girard [ab],
J.J. Gaardhøje [bv], M. Gagliardi [w], A. Gago [cr], M. Gallio [w], D.R. Gangadharan [r], P. Ganoti [bz], C. Garabatos [cl],
E. Garcia-Solis [l], C. Gargiulo [ag], I. Garishvili [bq], J. Gerhard [al], M. Germain [da], A. Gheata [ag], M. Gheata [ag,be],
B. Ghidini [ad], P. Ghosh [dq], P. Gianotti [bn], P. Giubellino [ag], E. Gladysz-Dziadus [dd], P. Glässel [ch], L. Goerlich [dd],
R. Gomez [j,df], P. González-Zamora [i], S. Gorbunov [al], S. Gotovac [dc], L.K. Graczykowski [ds], R. Grajcarek [ch],
A. Grelli [az], C. Grigoras [ag], A. Grigoras [ag], V. Grigoriev [br], A. Grigoryan [a], S. Grigoryan [bi], B. Grinyov [c],
N. Grion [cy], J.F. Grosse-Oetringhaus [ag], J.-Y. Grossiord [do], R. Grosso [ag], F. Guber [ay], R. Guernane [bm],
B. Guerzoni [y], M. Guilbaud [do], K. Gulbrandsen [bv], H. Gulkanyan [a], T. Gunji [dl], A. Gupta [cf], R. Gupta [cf],
K.H. Khan [n], R. Haake [av], Ø. Haaland [q], C. Hadjidakis [ar], M. Haiduc [be], H. Hamagaki [dl], G. Hamar [du],
L.D. Hanratty [cq], A. Hansen [bv], J.W. Harris [dv], H. Hartmann [al], A. Harton [l], D. Hatzifotiadou [ct], S. Hayashi [dl],
A. Hayrapetyan [ag,a], S.T. Heckel [at], M. Heide [av], H. Helstrup [ah], A. Herghelegiu [bt], G. Herrera Corral [j],
N. Herrmann [ch], B.A. Hess [af], K.F. Hetland [ah], B. Hicks [dv], B. Hippolyte [aw], Y. Hori [dl], P. Hristov [ag],
I. Hřivnáčová [ar], M. Huang [q], T.J. Humanic [r], D. Hutter [al], D.S. Hwang [s], R. Ilkaev [cn], I. Ilkiv [bs], M. Inaba [dm],
E. Incani [u], G.M. Innocenti [w], C. Ionita [ag], M. Ippolitov [co], M. Irfan [p], M. Ivanov [cl], V. Ivanov [ca],
O. Ivanytskyi [c], A. Jachołkowski [z], P.M. Jacobs [bp], C. Jahnke [dg], H.J. Jang [bj], M.A. Janik [ds],
P.H.S.Y. Jayarathna [di], S. Jena [ap,di], R.T. Jimenez Bustamante [bf], P.G. Jones [cq], H. Jung [am], A. Jusko [cq],
S. Kalcher [al], P. Kaliňák [bb], A. Kalweit [ag], J.H. Kang [dw], V. Kaplin [br], S. Kar [dq], A. Karasu Uysal [bk],
O. Karavichev [ay], T. Karavicheva [ay], E. Karpechev [ay], A. Kazantsev [co], U. Kebschull [as], R. Keidel [dx],
B. Ketzer [at], M.M. Khan [p], P. Khan [cp], S.A. Khan [dq], A. Khanzadeev [ca], Y. Kharlov [ax], B. Kileng [ah], T. Kim [dw],
B. Kim [dw], D.J. Kim [dj], D.W. Kim [am,bj], J.S. Kim [am], M. Kim [am], M. Kim [dw], S. Kim [s], S. Kirsch [al], I. Kisel [al],
S. Kiselev [ba], A. Kisiel [ds], G. Kiss [du], J.L. Klay [e], J. Klein [ch], C. Klein-Bösing [av], A. Kluge [ag], M.L. Knichel [cl],
A.G. Knospe [de], C. Kobdaj [ag,db], M.K. Köhler [cl], T. Kollegger [al], A. Kolojvari [dp], V. Kondratiev [dp],
N. Kondratyeva [br], A. Konevskikh [ay], V. Kovalenko [dp], M. Kowalski [dd], S. Kox [bm],
G. Koyithatta Meethaleveedu [ap], J. Kral [dj], I. Králik [bb], F. Kramer [at], A. Kravčáková [ak], M. Krelina [aj],
M. Kretz [al], M. Krivda [bb,cq], F. Krizek [aj,by,an], M. Krus [aj], E. Kryshen [ca], M. Krzewicki [cl], V. Kucera [by],
Y. Kucheriaev [co], T. Kugathasan [ag], C. Kuhn [aw], P.G. Kuijer [bw], I. Kulakov [at], J. Kumar [ap], P. Kurashvili [bs],
A.B. Kurepin [ay], A. Kurepin [ay], A. Kuryakin [cn], V. Kushpil [by], S. Kushpil [by], M.J. Kweon [ch], Y. Kwon [dw],
P. Ladrón de Guevara [bf], C. Lagana Fernandes [dg], I. Lakomov [ar], R. Langoy [dr], C. Lara [as], A. Lardeux [da],
A. Lattuca [w], S.L. La Pointe [az], P. La Rocca [z], R. Lea [v], M. Lechman [ag], S.C. Lee [am], G.R. Lee [cq], I. Legrand [ag],
J. Lehnert [at], R.C. Lemmon [bx], M. Lenhardt [cl], V. Lenti [cs], M. Leoncino [w], I. León Monzón [df], P. Lévai [du],
S. Li [bl,f], J. Lien [dr,q], R. Lietava [cq], S. Lindal [t], V. Lindenstruth [al], C. Lippmann [cl], M.A. Lisa [r],
H.M. Ljunggren [ae], D.F. Lodato [az], P.I. Loenne [q], V.R. Loggins [dt], V. Loginov [br], D. Lohner [ch], C. Loizides [bp],
X. Lopez [bl], E. López Torres [h], G. Løvhøiden [t], X.-G. Lu [ch], P. Luettig [at], M. Lunardon [aa], J. Luo [f],
G. Luparello [az], C. Luzzi [ag], R. Ma [dv], A. Maevskaya [ay], M. Mager [ag], D.P. Mahapatra [bd], A. Maire [ch],
M. Malaev [ca], I. Maldonado Cervantes [bf], L. Malinina [bi,1], D. Mal'Kevich [ba], P. Malzacher [cl], A. Mamonov [cn],
L. Manceau [cz], V. Manko [co], F. Manso [bl], V. Manzari [cs,ag], M. Marchisone [bl,w], J. Mareš [bc],
G.V. Margagliotti [v], A. Margotti [ct], A. Marín [cl], C. Markert [de,ag], M. Marquard [at], I. Martashvili [dk],
N.A. Martin [cl], P. Martinengo [ag], M.I. Martínez [b], G. Martínez García [da], J. Martin Blanco [da], Y. Martynov [c],
A. Mas [da], S. Masciocchi [cl], M. Masera [w], A. Masoni [cu], L. Massacrier [da], A. Mastroserio [ad], A. Matyja [dd],
J. Mazer [dk], R. Mazumder [aq], M.A. Mazzoni [cx], F. Meddi [x], A. Menchaca-Rocha [bg], J. Mercado Pérez [ch],
M. Meres [ai], Y. Miake [dm], K. Mikhaylov [bi,ba], L. Milano [ag,w], J. Milosevic [t,2], A. Mischke [az], A.N. Mishra [aq],
D. Miśkowiec [cl], C. Mitu [be], J. Mlynarz [dt], B. Mohanty [dq,bu], L. Molnar [aw,du], L. Montaño Zetina [j],
M. Monteno [cz], E. Montes [i], M. Morando [aa], D.A. Moreira De Godoy [dg], S. Moretto [aa], A. Morreale [dj],
A. Morsch [ag], V. Muccifora [bn], E. Mudnic [dc], S. Muhuri [dq], M. Mukherjee [dq], H. Müller [ag], M.G. Munhoz [dg],
S. Murray [bh], L. Musa [ag], B.K. Nandi [ap], R. Nania [ct], E. Nappi [cs], C. Nattrass [dk], T.K. Nayak [dq], S. Nazarenko [cn],
A. Nedosekin [ba], M. Nicassio [cl,ad], M. Niculescu [ag,be], B.S. Nielsen [bv], S. Nikolaev [co], S. Nikulin [co],
V. Nikulin [ca], B.S. Nilsen [cb], M.S. Nilsson [t], F. Noferini [k,ct], P. Nomokonov [bi], G. Nooren [az], A. Nyanin [co],

A. Nyatha [ap], J. Nystrand [q], H. Oeschler [ch,au], S.K. Oh [am,3], S. Oh [dv], L. Olah [du], J. Oleniacz [ds],
A.C. Oliveira Da Silva [dg], J. Onderwaater [cl], C. Oppedisano [cz], A. Ortiz Velasquez [ae], A. Oskarsson [ae],
J. Otwinowski [cl], K. Oyama [ch], Y. Pachmayer [ch], M. Pachr [aj], P. Pagano [ab], G. Paić [bf], F. Painke [al], C. Pajares [o],
S.K. Pal [dq], A. Palaha [cq], A. Palmeri [cv], V. Papikyan [a], G.S. Pappalardo [cv], W.J. Park [cl], A. Passfeld [av],
D.I. Patalakha [ax], V. Paticchio [cs], B. Paul [cp], T. Pawlak [ds], T. Peitzmann [az], H. Pereira Da Costa [m],
E. Pereira De Oliveira Filho [dg], D. Peresunko [co], C.E. Pérez Lara [bw], D. Perrino [ad], W. Peryt [ds,4], A. Pesci [ct],
Y. Pestov [d], V. Petráček [aj], M. Petran [aj], M. Petris [bt], P. Petrov [cq], M. Petrovici [bt], C. Petta [z], S. Piano [cy],
M. Pikna [ai], P. Pillot [da], O. Pinazza [ag,ct], L. Pinsky [di], N. Pitz [at], D.B. Piyarathna [di], M. Planinic [dn,cm],
M. Płoskoń [bp], J. Pluta [ds], S. Pochybova [du], P.L.M. Podesta-Lerma [df], M.G. Poghosyan [ag], B. Polichtchouk [ax],
A. Pop [bt], S. Porteboeuf-Houssais [bl], V. Pospíšil [aj], B. Potukuchi [cf], S.K. Prasad [dt], R. Preghenella [k,ct],
F. Prino [cz], C.A. Pruneau [dt], I. Pshenichnov [ay], G. Puddu [u], V. Punin [cn], J. Putschke [dt], H. Qvigstad [t],
A. Rachevski [cy], A. Rademakers [ag], J. Rak [dj], A. Rakotozafindrabe [m], L. Ramello [ac], S. Raniwala [cg],
R. Raniwala [cg], S.S. Räsänen [an], B.T. Rascanu [at], D. Rathee [cc], W. Rauch [ag], A.W. Rauf [n], V. Razazi [u],
K.F. Read [dk], J.S. Real [bm], K. Redlich [bs,5], R.J. Reed [dv], A. Rehman [q], P. Reichelt [at], M. Reicher [az], F. Reidt [ag,ch],
R. Renfordt [at], A.R. Reolon [bn], A. Reshetin [ay], F. Rettig [al], J.-P. Revol [ag], K. Reygers [ch], L. Riccati [cz],
R.A. Ricci [bo], T. Richert [ae], M. Richter [t], P. Riedler [ag], W. Riegler [ag], F. Riggi [z], A. Rivetti [cz],
M. Rodríguez Cahuantzi [b], A. Rodriguez Manso [bw], K. Røed [q,t], E. Rogochaya [bi], S. Rohni [cf], D. Rohr [al],
D. Röhrich [q], R. Romita [bx,cl], F. Ronchetti [bn], P. Rosnet [bl], S. Rossegger [ag], A. Rossi [ag], P. Roy [cp], C. Roy [aw],
A.J. Rubio Montero [i], R. Rui [v], R. Russo [w], E. Ryabinkin [co], A. Rybicki [dd], S. Sadovsky [ax], K. Šafařík [ag],
R. Sahoo [aq], P.K. Sahu [bd], J. Saini [dq], H. Sakaguchi [ao], S. Sakai [bp,bn], D. Sakata [dm], C.A. Salgado [o],
J. Salzwedel [r], S. Sambyal [cf], V. Samsonov [ca], X. Sanchez Castro [bf,aw], L. Šándor [bb], A. Sandoval [bg],
M. Sano [dm], G. Santagati [z], R. Santoro [k,ag], D. Sarkar [dq], E. Scapparone [ct], F. Scarlassara [aa],
R.P. Scharenberg [cj], C. Schiaua [bt], R. Schicker [ch], C. Schmidt [cl], H.R. Schmidt [af], S. Schuchmann [at],
J. Schukraft [ag], M. Schulc [aj], T. Schuster [dv], Y. Schutz [ag,da], K. Schwarz [cl], K. Schweda [cl], G. Scioli [y],
E. Scomparin [cz], R. Scott [dk], P.A. Scott [cq], G. Segato [aa], I. Selyuzhenkov [cl], J. Seo [ck], S. Serci [u],
E. Serradilla [i,bg], A. Sevcenco [be], A. Shabetai [da], G. Shabratova [bi], R. Shahoyan [ag], S. Sharma [cf], N. Sharma [dk],
K. Shigaki [ao], K. Shtejer [h], Y. Sibiriak [co], S. Siddhanta [cu], T. Siemiarczuk [bs], D. Silvermyr [bz], C. Silvestre [bm],
G. Simatovic [dn], R. Singaraju [dq], R. Singh [cf], S. Singha [dq], V. Singhal [dq], B.C. Sinha [dq], T. Sinha [cp], B. Sitar [ai],
M. Sitta [ac], T.B. Skaali [t], K. Skjerdal [q], R. Smakal [aj], N. Smirnov [dv], R.J.M. Snellings [az], R. Soltz [bq], M. Song [dw],
J. Song [ck], C. Soos [ag], F. Soramel [aa], M. Spacek [aj], I. Sputowska [dd], M. Spyropoulou-Stassinaki [cd],
B.K. Srivastava [cj], J. Stachel [ch], I. Stan [be], G. Stefanek [bs], M. Steinpreis [r], E. Stenlund [ae], G. Steyn [bh],
J.H. Stiller [ch], D. Stocco [da], M. Stolpovskiy [ax], P. Strmen [ai], A.A.P. Suaide [dg], M.A. Subieta Vásquez [w],
T. Sugitate [ao], C. Suire [ar], M. Suleymanov [n], R. Sultanov [ba], M. Šumbera [by], T. Susa [cm], T.J.M. Symons [bp],
A. Szanto de Toledo [dg], I. Szarka [ai], A. Szczepankiewicz [ag], M. Szymański [ds], J. Takahashi [dh],
M.A. Tangaro [ad], J.D. Tapia Takaki [ar], A. Tarantola Peloni [at], A. Tarazona Martinez [ag], A. Tauro [ag],
G. Tejeda Muñoz [b], A. Telesca [ag], C. Terrevoli [ad], A. Ter Minasyan [co,br], J. Thäder [cl], D. Thomas [az],
R. Tieulent [do], A.R. Timmins [di], A. Toia [cw], H. Torii [dl], V. Trubnikov [c], W.H. Trzaska [dj], T. Tsuji [dl],
A. Tumkin [cn], R. Turrisi [cw], T.S. Tveter [t], J. Ulery [at], K. Ullaland [q], J. Ulrich [as], A. Uras [do], G.M. Urciuoli [cx],
G.L. Usai [u], M. Vajzer [by], M. Vala [bb,bi], L. Valencia Palomo [ar], P. Vande Vyvre [ag], L. Vannucci [bo],
J.W. Van Hoorne [ag], M. van Leeuwen [az], A. Vargas [b], R. Varma [ap], M. Vasileiou [cd], A. Vasiliev [co],
V. Vechernin [dp], M. Veldhoen [az], M. Venaruzzo [v], E. Vercellin [w], S. Vergara [b], R. Vernet [g], M. Verweij [dt,az],
L. Vickovic [dc], G. Viesti [aa], J. Viinikainen [dj], Z. Vilakazi [bh], O. Villalobos Baillie [cq], A. Vinogradov [co],
L. Vinogradov [dp], Y. Vinogradov [cn], T. Virgili [ab], Y.P. Viyogi [dq], A. Vodopyanov [bi], M.A. Völkl [ch],
S. Voloshin [dt], K. Voloshin [ba], G. Volpe [ag], B. von Haller [ag], I. Vorobyev [dp], D. Vranic [ag,cl], J. Vrláková [ak],
B. Vulpescu [bl], A. Vyushin [cn], B. Wagner [q], V. Wagner [aj], J. Wagner [cl], Y. Wang [ch], Y. Wang [f], M. Wang [f],
D. Watanabe [dm], K. Watanabe [dm], M. Weber [di], J.P. Wessels [av], U. Westerhoff [av], J. Wiechula [af], J. Wikne [t],
M. Wilde [av], G. Wilk [bs], J. Wilkinson [ch], M.C.S. Williams [ct], B. Windelband [ch], M. Winn [ch], C. Xiang [f],
C.G. Yaldo [dt], Y. Yamaguchi [dl], H. Yang [m,az], P. Yang [f], S. Yang [q], S. Yano [ao], S. Yasnopolskiy [co], J. Yi [ck],
Z. Yin [f], I.-K. Yoo [ck], I. Yushmanov [co], V. Zaccolo [bv], C. Zach [aj], C. Zampolli [ct], S. Zaporozhets [bi],
A. Zarochentsev [dp], P. Závada [bc], N. Zaviyalov [cn], H. Zbroszczyk [ds], P. Zelnicek [as], I.S. Zgura [be], M. Zhalov [ca],
F. Zhang [f], Y. Zhang [f], H. Zhang [f], X. Zhang [bp,bl,f], D. Zhou [f], Y. Zhou [az], F. Zhou [f], X. Zhu [f], J. Zhu [f], J. Zhu [f],

H. Zhu [f], A. Zichichi [k,y], M.B. Zimmermann [av,ag], A. Zimmermann [ch], G. Zinovjev [c], Y. Zoccarato [do], M. Zynovyev [c], M. Zyzak [at]

[a] *A.I. Alikhanyan National Science Laboratory (Yerevan Physics Institute) Foundation, Yerevan, Armenia*
[b] *Benemérita Universidad Autónoma de Puebla, Puebla, Mexico*
[c] *Bogolyubov Institute for Theoretical Physics, Kiev, Ukraine*
[d] *Budker Institute for Nuclear Physics, Novosibirsk, Russia*
[e] *California Polytechnic State University, San Luis Obispo, CA, United States*
[f] *Central China Normal University, Wuhan, China*
[g] *Centre de Calcul de l'IN2P3, Villeurbanne, France*
[h] *Centro de Aplicaciones Tecnológicas y Desarrollo Nuclear (CEADEN), Havana, Cuba*
[i] *Centro de Investigaciones Energéticas Medioambientales y Tecnológicas (CIEMAT), Madrid, Spain*
[j] *Centro de Investigación y de Estudios Avanzados (CINVESTAV), Mexico City and Mérida, Mexico*
[k] *Centro Fermi – Museo Storico della Fisica e Centro Studi e Ricerche "Enrico Fermi", Rome, Italy*
[l] *Chicago State University, Chicago, United States*
[m] *Commissariat à l'Energie Atomique, IRFU, Saclay, France*
[n] *COMSATS Institute of Information Technology (CIIT), Islamabad, Pakistan*
[o] *Departamento de Física de Partículas and IGFAE, Universidad de Santiago de Compostela, Santiago de Compostela, Spain*
[p] *Department of Physics, Aligarh Muslim University, Aligarh, India*
[q] *Department of Physics and Technology, University of Bergen, Bergen, Norway*
[r] *Department of Physics, Ohio State University, Columbus, OH, United States*
[s] *Department of Physics, Sejong University, Seoul, South Korea*
[t] *Department of Physics, University of Oslo, Oslo, Norway*
[u] *Dipartimento di Fisica dell'Università and Sezione INFN, Cagliari, Italy*
[v] *Dipartimento di Fisica dell'Università and Sezione INFN, Trieste, Italy*
[w] *Dipartimento di Fisica dell'Università and Sezione INFN, Turin, Italy*
[x] *Dipartimento di Fisica dell'Università 'La Sapienza' and Sezione INFN, Rome, Italy*
[y] *Dipartimento di Fisica e Astronomia dell'Università and Sezione INFN, Bologna, Italy*
[z] *Dipartimento di Fisica e Astronomia dell'Università and Sezione INFN, Catania, Italy*
[aa] *Dipartimento di Fisica e Astronomia dell'Università and Sezione INFN, Padova, Italy*
[ab] *Dipartimento di Fisica 'E.R. Caianiello' dell'Università and Gruppo Collegato INFN, Salerno, Italy*
[ac] *Dipartimento di Scienze e Innovazione Tecnologica dell'Università del Piemonte Orientale and Gruppo Collegato INFN, Alessandria, Italy*
[ad] *Dipartimento Interateneo di Fisica 'M. Merlin' and Sezione INFN, Bari, Italy*
[ae] *Division of Experimental High Energy Physics, University of Lund, Lund, Sweden*
[af] *Eberhard Karls Universität Tübingen, Tübingen, Germany*
[ag] *European Organization for Nuclear Research (CERN), Geneva, Switzerland*
[ah] *Faculty of Engineering, Bergen University College, Bergen, Norway*
[ai] *Faculty of Mathematics, Physics and Informatics, Comenius University, Bratislava, Slovakia*
[aj] *Faculty of Nuclear Sciences and Physical Engineering, Czech Technical University in Prague, Prague, Czech Republic*
[ak] *Faculty of Science, P.J. Šafárik University, Košice, Slovakia*
[al] *Frankfurt Institute for Advanced Studies, Johann Wolfgang Goethe-Universität Frankfurt, Frankfurt, Germany*
[am] *Gangneung-Wonju National University, Gangneung, South Korea*
[an] *Helsinki Institute of Physics (HIP), Helsinki, Finland*
[ao] *Hiroshima University, Hiroshima, Japan*
[ap] *Indian Institute of Technology Bombay (IIT), Mumbai, India*
[aq] *Indian Institute of Technology Indore (IITI), India*
[ar] *Institut de Physique Nucléaire d'Orsay (IPNO), Université Paris-Sud, CNRS–IN2P3, Orsay, France*
[as] *Institut für Informatik, Johann Wolfgang Goethe-Universität Frankfurt, Frankfurt, Germany*
[at] *Institut für Kernphysik, Johann Wolfgang Goethe-Universität Frankfurt, Frankfurt, Germany*
[au] *Institut für Kernphysik, Technische Universität Darmstadt, Darmstadt, Germany*
[av] *Institut für Kernphysik, Westfälische Wilhelms-Universität Münster, Münster, Germany*
[aw] *Institut Pluridisciplinaire Hubert Curien (IPHC), Université de Strasbourg, CNRS–IN2P3, Strasbourg, France*
[ax] *Institute for High Energy Physics, Protvino, Russia*
[ay] *Institute for Nuclear Research, Academy of Sciences, Moscow, Russia*
[az] *Institute for Subatomic Physics of Utrecht University, Utrecht, Netherlands*
[ba] *Institute for Theoretical and Experimental Physics, Moscow, Russia*
[bb] *Institute of Experimental Physics, Slovak Academy of Sciences, Košice, Slovakia*
[bc] *Institute of Physics, Academy of Sciences of the Czech Republic, Prague, Czech Republic*
[bd] *Institute of Physics, Bhubaneswar, India*
[be] *Institute of Space Science (ISS), Bucharest, Romania*
[bf] *Instituto de Ciencias Nucleares, Universidad Nacional Autónoma de México, Mexico City, Mexico*
[bg] *Instituto de Física, Universidad Nacional Autónoma de México, Mexico City, Mexico*
[bh] *iThemba LABS, National Research Foundation, Somerset West, South Africa*
[bi] *Joint Institute for Nuclear Research (JINR), Dubna, Russia*
[bj] *Korea Institute of Science and Technology Information, Daejeon, South Korea*
[bk] *KTO Karatay University, Konya, Turkey*
[bl] *Laboratoire de Physique Corpusculaire (LPC), Clermont Université, Université Blaise Pascal, CNRS–IN2P3, Clermont-Ferrand, France*
[bm] *Laboratoire de Physique Subatomique et de Cosmologie (LPSC), Université Joseph Fourier, CNRS–IN2P3, Institut Polytechnique de Grenoble, Grenoble, France*
[bn] *Laboratori Nazionali di Frascati, INFN, Frascati, Italy*
[bo] *Laboratori Nazionali di Legnaro, INFN, Legnaro, Italy*
[bp] *Lawrence Berkeley National Laboratory, Berkeley, CA, United States*
[bq] *Lawrence Livermore National Laboratory, Livermore, CA, United States*
[br] *Moscow Engineering Physics Institute, Moscow, Russia*
[bs] *National Centre for Nuclear Studies, Warsaw, Poland*
[bt] *National Institute for Physics and Nuclear Engineering, Bucharest, Romania*
[bu] *National Institute of Science Education and Research, Bhubaneswar, India*
[bv] *Niels Bohr Institute, University of Copenhagen, Copenhagen, Denmark*
[bw] *Nikhef, National Institute for Subatomic Physics, Amsterdam, Netherlands*

[bx] *Nuclear Physics Group, STFC Daresbury Laboratory, Daresbury, United Kingdom*
[by] *Nuclear Physics Institute, Academy of Sciences of the Czech Republic, Řež u Prahy, Czech Republic*
[bz] *Oak Ridge National Laboratory, Oak Ridge, TN, United States*
[ca] *Petersburg Nuclear Physics Institute, Gatchina, Russia*
[cb] *Physics Department, Creighton University, Omaha, NE, United States*
[cc] *Physics Department, Panjab University, Chandigarh, India*
[cd] *Physics Department, University of Athens, Athens, Greece*
[ce] *Physics Department, University of Cape Town, Cape Town, South Africa*
[cf] *Physics Department, University of Jammu, Jammu, India*
[cg] *Physics Department, University of Rajasthan, Jaipur, India*
[ch] *Physikalisches Institut, Ruprecht-Karls-Universität Heidelberg, Heidelberg, Germany*
[ci] *Politecnico di Torino, Turin, Italy*
[cj] *Purdue University, West Lafayette, IN, United States*
[ck] *Pusan National University, Pusan, South Korea*
[cl] *Research Division and ExtreMe Matter Institute EMMI, GSI Helmholtzzentrum für Schwerionenforschung, Darmstadt, Germany*
[cm] *Rudjer Bošković Institute, Zagreb, Croatia*
[cn] *Russian Federal Nuclear Center (VNIIEF), Sarov, Russia*
[co] *Russian Research Centre Kurchatov Institute, Moscow, Russia*
[cp] *Saha Institute of Nuclear Physics, Kolkata, India*
[cq] *School of Physics and Astronomy, University of Birmingham, Birmingham, United Kingdom*
[cr] *Sección Física, Departamento de Ciencias, Pontificia Universidad Católica del Perú, Lima, Peru*
[cs] *Sezione INFN, Bari, Italy*
[ct] *Sezione INFN, Bologna, Italy*
[cu] *Sezione INFN, Cagliari, Italy*
[cv] *Sezione INFN, Catania, Italy*
[cw] *Sezione INFN, Padova, Italy*
[cx] *Sezione INFN, Rome, Italy*
[cy] *Sezione INFN, Trieste, Italy*
[cz] *Sezione INFN, Turin, Italy*
[da] *SUBATECH, Ecole des Mines de Nantes, Université de Nantes, CNRS–IN2P3, Nantes, France*
[db] *Suranaree University of Technology, Nakhon Ratchasima, Thailand*
[dc] *Technical University of Split FESB, Split, Croatia*
[dd] *The Henryk Niewodniczanski Institute of Nuclear Physics, Polish Academy of Sciences, Cracow, Poland*
[de] *The University of Texas at Austin, Physics Department, Austin, TX, United States*
[df] *Universidad Autónoma de Sinaloa, Culiacán, Mexico*
[dg] *Universidade de São Paulo (USP), São Paulo, Brazil*
[dh] *Universidade Estadual de Campinas (UNICAMP), Campinas, Brazil*
[di] *University of Houston, Houston, TX, United States*
[dj] *University of Jyväskylä, Jyväskylä, Finland*
[dk] *University of Tennessee, Knoxville, TN, United States*
[dl] *University of Tokyo, Tokyo, Japan*
[dm] *University of Tsukuba, Tsukuba, Japan*
[dn] *University of Zagreb, Zagreb, Croatia*
[do] *Université de Lyon, Université Lyon 1, CNRS/IN2P3, IPN-Lyon, Villeurbanne, France*
[dp] *V. Fock Institute for Physics, St. Petersburg State University, St. Petersburg, Russia*
[dq] *Variable Energy Cyclotron Centre, Kolkata, India*
[dr] *Vestfold University College, Tonsberg, Norway*
[ds] *Warsaw University of Technology, Warsaw, Poland*
[dt] *Wayne State University, Detroit, MI, United States*
[du] *Wigner Research Centre for Physics, Hungarian Academy of Sciences, Budapest, Hungary*
[dv] *Yale University, New Haven, CT, United States*
[dw] *Yonsei University, Seoul, South Korea*
[dx] *Zentrum für Technologietransfer und Telekommunikation (ZTT), Fachhochschule Worms, Worms, Germany*

[1] M.V. Lomonosov Moscow State University, D.V. Skobeltsyn Institute of Nuclear Physics, Moscow, Russia.
[2] University of Belgrade, Faculty of Physics and "Vinča" Institute of Nuclear Sciences, Belgrade, Serbia.
[3] Konkuk University, Seoul, Republic of Korea.
[4] Deceased.
[5] Institute of Theoretical Physics, University of Wroclaw, Wroclaw, Poland.